JBC MINIREVIEW

Metalloriboswitches: RNA-based inorganic ion sensors that regulate genes

Published, Papers in Press, April 28, 2017, DOI 10.1074/jbc.R117.787713

Joseph E. Wedekind[1], **Debapratim Dutta, Ivan A. Belashov, and Jermaine L. Jenkins**

From the Department of Biochemistry & Biophysics and Center for RNA Biology, University of Rochester School of Medicine and Dentistry, Rochester, New York 14642

Edited by F. Peter Guengerich

Divalent ions fulfill essential cellular roles and are required for virulence by certain bacteria. Free intracellular Mg^{2+} can approach 5 mM, but at this level Mn^{2+}, Ni^{2+}, or Co^{2+} can be growth-inhibitory, and magnesium fluoride is toxic. To maintain ion homeostasis, many bacteria have evolved ion sensors embedded in the 5′-leader sequences of mRNAs encoding ion uptake or efflux channels. Here, we review current insights into these "metalloriboswitches," emphasizing ion-specific binding by structured RNA aptamers and associated conformational changes in downstream signal sequences. This riboswitch-effector interplay produces a layer of gene regulatory feedback that has elicited interest as an antibacterial target.

Riboswitches are highly structured RNA motifs often located in the 5′-leader sequences of bacterial mRNAs (1–3). A riboswitch recognizes its cognate effector by a conserved aptamer domain, which elicits conformational changes in a downstream expression platform that alter transcription termination, translation initiation, message stability, or alternative splicing of the associated transcript (2, 4, 5). Because riboswitches evolved distinct molecular determinants to bind specific effectors, they have garnered interest not only for their elegant feedback mechanisms, but also for their potential to serve as novel drug targets. A prime example is the flavin mononucleotide (FMN) riboswitch, which can be inhibited by natural or synthetic ligand analogs that blunt the essential biosynthesis of riboflavin in bacteria (6–10). At present, nearly 40 riboswitch classes that recognize >25 chemically distinct effectors have been described (11), providing many opportunities to interrupt key anabolic pathways. Conversely, a growing cohort of riboswitches activate genes involved in remediation of cellular toxins, such as *S*-adenosylhomocysteine (12), azaaromatics (13), guanidine (14), Mg^{2+} (15), transition metals (16–18), or magnesium fluoride (19). Here, we discuss the latter three classes of riboswitches that evolved elegant but distinct RNA folds to recognize specific divalent cations, leading to gene-regulatory changes that maintain cellular homeostasis. In some cases, metalloriboswitch affinity and cooperativity can rival that of proteins. Many excellent riboswitch reviews provide broad overviews of the field (2, 3, 11). As such, we focus here on the handful of known metalloriboswitches with an emphasis on their discovery, validation, specificity, and gene regulation, as well as their potential to serve as drug targets.

Mg^{2+}-I riboswitches are non-specific sensors that regulate Mg^{2+} import pumps

Mg^{2+} is the most abundant intracellular, multivalent ion with free concentrations in bacteria ranging from 1 to 5 mM (20). Although numerous enzymes require Mg^{2+} for catalysis, the ion can also fulfill structural roles by neutralizing charged DNA or RNA backbones or acting as a nexus for functional group coordination in RNA tertiary structure (21, 22). The *Escherichia coli* 70S ribosome has ~170 coordinated Mg^{2+} ions (23), and the lack of Mg^{2+} in growth media leads to subunit dissolution and degradation (20). As a rule, bacteria employ a broad range of metallosensors and transporters to attain metal ion homeostasis (24). Some bacteria link Mg^{2+} concentration to virulence genes to coordinate gene expression in cation-deficient host cells, such as macrophages (25). *Salmonella enterica* has three Mg^{2+} importers: the widespread CorA channel and P-type ATPases MgtA and MgtB (26, 27). Recent salmonellosis outbreaks caused by the Heidelberg serovar are alarming due to the multidrug resistance of this organism (28, 29). In this and many other Gram-negative bacteria, *mgtA* expression is controlled by an upstream Mg^{2+}-sensing riboswitch (known as the Mg^{2+}-II class (11)) that regulates transcription via rho-dependent and RNase E degradation mechanisms (30–32). An additional level of control appears to be exerted by a proline-rich open reading frame inside the *mgtA* riboswitch that works in concert with Mg^{2+}-sensing to increase *mgtA* mRNA levels when Mg^{2+} is low (33, 34). Additional studies are needed to clarify the details of regulation, which appears to be present in only a handful of γ-proteobacteria (11). A second class of Mg^{2+}-sensing riboswitch known as the Mg^{2+}-I (or M-box) is more broadly distributed in Gram-positive and some Gram-negative bacteria, where it is controls a variety of genes (15, 25), including the widespread Mg^{2+}-uptake channel *mgtE* (27). In *Aeromonas hydrophila*, *mgtE* mutations impair swarming and biofilm formation (35), which are important aspects of its pathogenicity. The defined Mg^{2+}-I aptamer domain and readily discernible expression platform make it a model system

This work was supported in part by National Institutes of Health Grant GM063162 from NIGMS (to J. E. W.). The authors declare that they have no conflicts of interest with the contents of this article. The content is solely the responsibility of the authors and does not necessarily represent the official views of the National Institutes of Health.

[1] To whom correspondence should be addressed: Dept. Biochemistry and Biophysics and Center for RNA Biology, University of Rochester Medical Center, 601 Elmwood Ave., Box 712, Rochester, NY 14642. Tel.: 585-273-4516; Fax: 585-275-6007; E-mail: joseph.wedekind@rochester.edu.

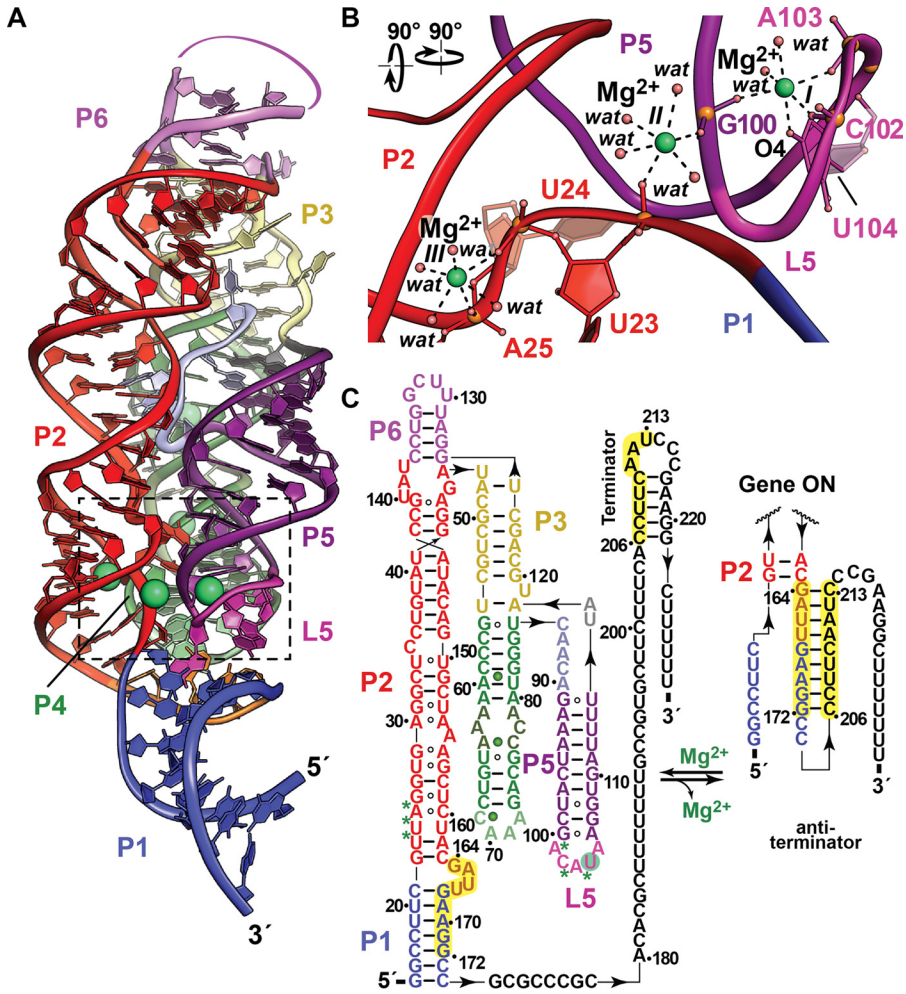

Figure 1. Tertiary fold and ion coordination by the Mg^{2+}-I riboswitch in the Mg^{2+}-bound state. *a,* ribbon diagram of the *B. subtilis* Mg^{2+}-I riboswitch co-crystal structure determined at 2.7 Å resolution (Protein Data Bank entry 2QBZ). The riboswitch fold contains three parallel helical domains, P1-P2-P6, P3-P4, and P5, wherein the former two segments coaxially stack. Four coordinated Mg^{2+} ions are depicted as *green spheres* at the interface of helices P1, P2, and P5 (foreground) and in P4 (background). *b,* close-up view of three Mg^{2+}-binding sites (I–III, *boxed* in *a*). The metal ions at each site coordinate in an octahedral manner. The site I Mg^{2+} is coordinated by the non-bridging phosphate oxygens of G100, C102, and A103. A fourth ligand is contributed by the O4 keto moiety of U104 with two inner-shell water molecules completing the coordination sphere. Site II uses non-bridging oxygens from G100 and U23 with the remaining coordination sphere completed by waters. Site III uses two non-bridging oxygens from U24 and A25, as well as four inner-sphere waters. *c,* secondary structure depicting changes in conformational states that regulate transcription. Paired regions are colored as in *a* with backbone binding contributions to Mg^{2+} from sites I–III depicted as *green asterisks*; additional Mg^{2+} sites in P4 are depicted as *green spheres*. In the gene-off state, Mg^{2+} binding at sites I–III promotes a conformation that destabilizes anti-terminator base pairing between the P1-P2 bulged loop (164–172) and the 3′-tail (206–213), favoring intrinsic-terminator hairpin formation that attenuates *mgtE* transcription, reducing Mg^{2+} uptake by the MgtE channel. Conversely, low Mg^{2+} favors RNA polymerase transcriptional read-through via an anti-terminator helix in place of P1. The full-length message leads to MgtE translation with increased Mg^{2+} import into the cell.

for structure and function analysis, which provides a benchmark for additional comparisons herein.

The aptamer of the Mg^{2+}-I riboswitch is not selective for Mg^{2+}, unlike other metal-sensing riboswitches (see below), as shown by the variety of divalent ions that promote compaction of its fold and favor formation of a downstream intrinsic terminator hairpin within the expression platform (15, 36). In this respect, Mg^{2+}-I riboswitches likely function by sensing the most prevalent intracellular ion, Mg^{2+}, which requires only modest affinity and selectivity, as corroborated by EC_{50} values of 0.4 mM for Mg^{2+} or Ca^{2+} and 0.13 mM for Mn^{2+} (36). Thus, Mg^{2+}-I riboswitches promote homeostasis but are outperformed by regulatory metalloproteins in terms of selectivity (16). To investigate the metal-binding determinants, structures of the Mg^{2+}-I riboswitch were determined in Mg^{2+}- and Mn^{2+}-bound states (15, 36). The global architecture features three parallel helical domains comprising P1-P2-P6, P3-P4, and P5 (Fig. 1*a*). Tertiary interactions are stabilized by six Mg^{2+} ions that promote compaction as shown biochemically (37). Four key Mg^{2+} sites (I–IV) reside at the P1-P2-P5 interface, whereas sites V and VI are in the P4 internal loop. The former metal constellation (core 1) contributes to interhelical tertiary stability, whereas the latter (core 2) appears to orient the P4 loop to facilitate long-range contacts (36). Biochemical evidence also supports additional Mg^{2+} binding, but these sites (core 3) were visible only in structures obtained from crystals grown from 5 mM Mn^{2+}, which was used as a proxy for Mg^{2+}. Importantly, only core 1 ions were present in all structures, including crystal forms harboring multiple Mg^{2+}-I riboswitch copies per asymmetric unit. Moreover, sites I–III exhibited the highest phosphorothioate interference (37) with superimposable Mg^{2+} and Mn^{2+} coordination in pairwise structural com-

parisons (36). As such, it is worthwhile to describe these strong binding sites with a focus on how their tertiary contacts at these locations relate to gene regulatory conformations.

The site I Mg^{2+} is coordinated by non-bridging phosphate oxygens at the transition of P5 into L5 with a fourth ligand contributed by the U104 base (Fig. 1*b*). Site II also uses non-bridging oxygens from P5 and P2 with the remaining coordination sphere completed by waters. Likewise, site III comprises two non-bridging oxygens from P2 and four waters. Shared coordination groups, such as the phosphate of G100, provide a plausible basis for cooperativity between Mg^{2+}-binding sites (Hill coefficient 4.3) (36), which confers a sharp "digital" response to the effector over a narrow concentration range.

Gene regulation by the Mg^{2+}-I riboswitch is predicated on Mg^{2+}-mediated condensation of the RNA fold (Fig. 1*a*) that favors sequestration of an anti-terminator sequence (164–172) located between P1 and P2 (Fig. 1*c*). This effector-bound conformation promotes an alternate, intrinsic terminator harboring the 3′-anti-terminator sequence (206–213), thus blocking transcription of the downstream *mgtE* gene, leading to attenuated Mg^{2+} uptake by a diminished population of MgtE channels. Conversely, depleted cellular Mg^{2+} alters the interface between P1-P2 and P5-L5 (sites I–III), promoting formation of an anti-terminator hairpin (Fig. 1*c*) that favors full-length *mgtE* transcription, resulting in Mg^{2+} import. The presence of distinct Mg^{2+}-sensing riboswitches in human pathogens suggests that these RNA elements could be targets for antibacterials, especially because the associated Mg^{2+} transport genes are linked to virulence (discussed below).

Orphan riboswitch *yybP-ykoY* senses Mn^{2+} to activate intake pumps

Manganese is an essential trace element that plays key cellular roles, including facilitating the catalytic activity of various ribonucleotide reductases and superoxide dismutases expressed under low iron conditions or H_2O_2 stress (38). Bacteria exhibit varied Mn^{2+} requirements that reflect survival adaptations to specific microenvironments. *E. coli* can tolerate up to 20 mM Mn^{2+} (39) but maintains cellular levels at ~1 μM (24), whereas *Bacillus subtilis* has cytosolic levels of ~10 μM (40). For some bacteria, Mn^{2+} is toxic because in various enzymes it replaces Fe^{2+}, which is not tolerated functionally (38). Conversely, *Borrelia* and *Lactobacillus* are members of small bacterial cohorts that use Mn^{2+} with preference over iron (41, 42), a strategy that bypasses host efforts to restrict iron levels, at least in the former case. Likewise, mutations in the macrophage-specific natural resistance-associated macrophage protein 1 (Nramp1) transporter–a Mn^{2+}, Fe^{2+}, and Zn^{2+} uptake antiporter–led to diminished host resistance against *Salmonella*, *Leishmania,* and *Mycobacterium* (43), possibly resulting from a reduced capacity to remove divalent cations from bacteria-containing vacuoles in the host (44). Conversely, bacterial virulence can be attenuated by mutation of Nramp1 homologs of the pathogen, linking virulence to Mn^{2+} uptake. *Salmonella* uses Mn^{2+} transporters MntH (an Nramp1 homolog) and SitABCD (an ATP-binding cassette protein) (45), and a *typhimurium* serovar lacking both is avirulent (46). The *mntH* and *sitABCD* genes are repressed by the *trans*-acting Fur and MntR proteins in high Mn^{2+}, although an additional *cis*-acting Mn^{2+}-responsive riboswitch is hypothesized to reside in the 5′-leader of *Salmonella mntH* genes (47). This element requires further validation, but it ostensibly favors anti-terminator stem formation at low Mn^{2+} concentrations, leading to MntH expression and Mn^{2+} uptake. Exporters of Mn^{2+} are also required by bacteria to attain homeostasis. The finding that the *mntP* (formerly *yebN*) encodes Mn^{2+} efflux pumps, and is controlled by the Mn^{2+}-responsive Fur and MntR proteins (48–50), provided insight into a longstanding riboswitch mystery. The ubiquitous *yybP-ykoY* RNA motif, classified for years as an "orphan" riboswitch for lack of a known effector (51, 52), was identified in the 5′-leaders of *mntP* genes, suggesting that Mn^{2+} was the long-sought ligand (17, 18). Indeed, independent labs validated the *yybP-ykoY* or Mn^{2+} riboswitch as an Mn^{2+} sensor that controls expression of a P-type uptake pump (17, 18). This provided a firm basis to understand how a metalloriboswitch discriminates between Mg^{2+} and Mn^{2+}, leading to cellular resistance against the toxic effects of a transition metal.

A structure of the Mn^{2+} riboswitch revealed a four-way helical junction comprising tandem coaxially stacked helices (Fig. 2*a*). Mn^{2+}-induced fold compaction based on chemical modification showed reduced loop flexibility at L1 and L3 and the base of P1 (17) with reactivity changes at U87 and A88 producing a $K_{D,\,app}$ value for Mn^{2+} of 27 $\pm$ 6 μM. Chemical mapping also corroborated the structure, wherein two divalent ion-binding sites localize in bulged loops L1 and L3 to compose a prominent tertiary docking interface at the helical junction (Fig. 2, *a* and *b*). At site I, Mn^{2+} is coordinated by the N7 moiety of A41 and non-bridging phosphate oxygens from L3 and L1. The nearby site II pocket binds Mg^{2+} using only oxygen atoms contributed by non-bridging groups of L1 and L3, as well as a single water molecule, consistent with the recalcitrance of $Mg(H_2O)_6{}^{2+}$ to release its inner-sphere waters (53). Regarding the basis of Mn^{2+} selectivity at site I, it is notable that Mn^{2+} exhibits a more polarizable (softer) character in high-coordination-number environments, whereas Mg^{2+} is oxophilic (harder) with less preference for nitrogen (53). Nonetheless, Mn^{2+} functionally substitutes for Mg^{2+} in many enzymes, and octahedral Mg^{2+} will coordinate nitrogen (53). Consistent with these findings, riboswitch crystals prepared from 2.5 mM Mn^{2+} incorporated Mn^{2+} at both binding sites (17), but only site I was occupied when the Mn^{2+} concentration was reduced to 100 μM. Although biochemical cooperativity was not analyzed, interdependence of the ion-binding sites is likely based on shared coordination of non-bridging phosphate oxygens (Fig. 2*b*). As anticipated, 41A→U and 41A→G mutations are less responsive to Mn^{2+} and are accompanied by enhanced L3 flexibility, consistent with rearrangement of the coordination pocket. It has been noted for proteins that insertion of a single nitrogen into a coordination sphere can exclude Mg^{2+} and favor Mn^{2+} (53). As such, it is reasonable that N7 of conserved A41 is a major selectivity determinant for Mn^{2+} in the Mn^{2+} riboswitch, which could account for the ability of Mn^{2+} to bind even in the presence of relatively high Mg^{2+} ion levels in the cytosol.

Gene regulation by Mn^{2+} riboswitches occurs by two distinct mechanisms involving transcriptional and translational

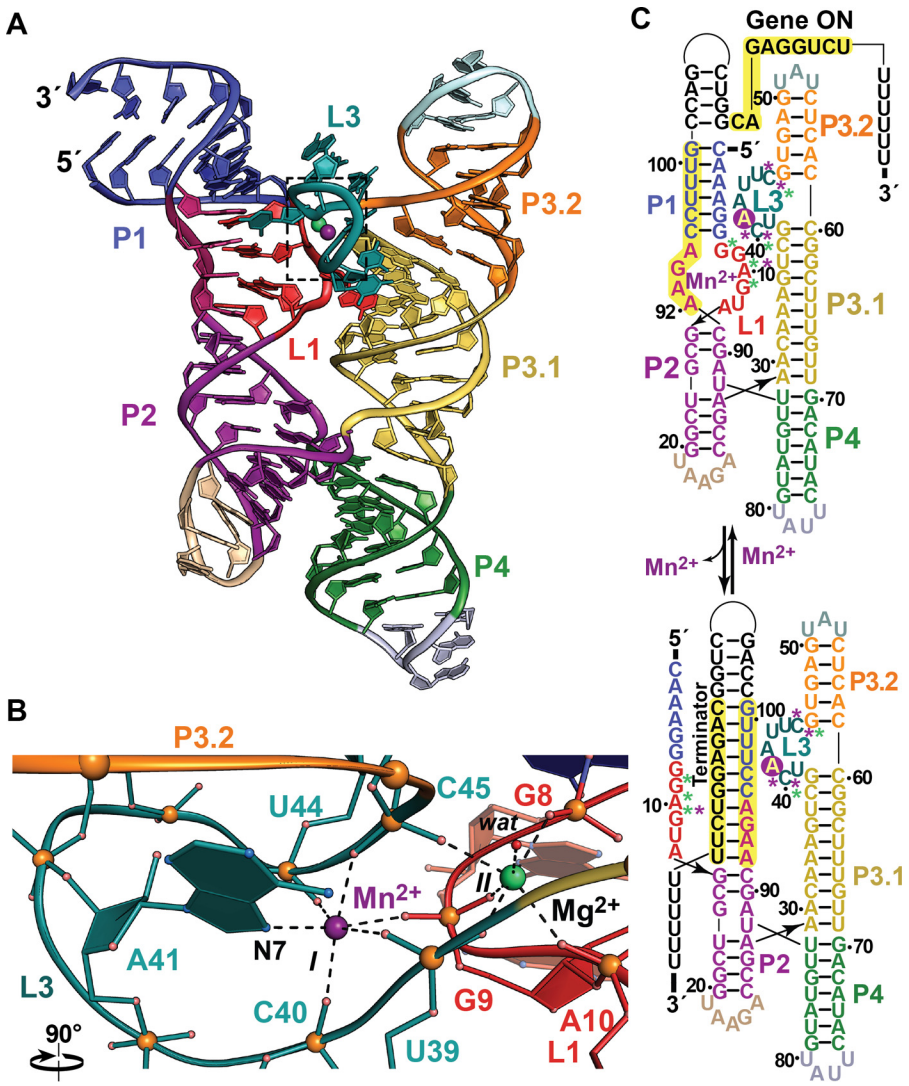

Figure 2. Tertiary fold and ion coordination by the Mn^{2+} riboswitch bound to Mn^{2+} and Mg^{2+}. *a,* ribbon diagram of the *Lactococcus lactis* Mn^{2+} riboswitch co-crystal structure determined at 2.85 Å resolution (Protein Data Bank entry 4Y1I) showing a four-way helical junction containing parallel, coaxially stacked helices P1-P2 and P3-P4. Divalent ion recognition occurs at the helical junction between loops L1 and L3, where Mn^{2+} (site I, *magenta*) and Mg^{2+} (site II, *green*) bind. *b,* close-up view of the octahedral divalent ion coordination at sites I and II (*boxed* in *a*). Mn^{2+} is observed at site I and is preferred over Mg^{2+} based on the N7 group of the A41 base. Non-bridging phosphate oxygens are contributed from U39, C40, U44, and C45 of L3, as well as G9 of L1. Site II is coordinated by non-bridging oxygens of G8, G9, and A10 of L1 and U39 and C45 of L3; an inner-sphere water molecule completes the coordination shell. Each non-bridging phosphate oxygen of G9 contributes to ion binding at sites I and II, providing a basis for cooperative binding. *c,* secondary structure diagrams depicting changes in Mn^{2+} riboswitch conformational states that regulate transcription. Backbone contributions to Mn^{2+} and Mg^{2+} binding are depicted as *magenta* and *green asterisks*; Mn^{2+} coordination at N7 of A41 is depicted as a *magenta circle*. In the gene-on state, Mn^{2+} and Mg^{2+} binding at sites I and II promote a conformation that facilitates base pairing of an anti-terminator hairpin above P1, favoring transcription of the *mntP* (*yoaB*) efflux pump that confers Mn^{2+} resistance. Conversely, low Mn^{2+} levels favor formation of an intrinsic terminator hairpin at the expense of the P1 helix and the L1-L3 ion-binding sites. A premature *mntP* (*yoaB*) message leads to reduced expression of the associated Mn^{2+} efflux channel.

control (17, 18). Structural analysis of the *E. coli* riboswitch showed that site I collapses in the absence of Mn^{2+}, whereas site II remains intact and occupied by Mg^{2+} (17). However, Mg^{2+} alone did not stabilize the L1-L3 binding interface in chemical-modification experiments, which has implications for formation of mutually exclusive expression platform conformations that regulate transcription. At high Mn^{2+} concentrations, the L1-L3 interface is well ordered (Fig. 2*b*), giving rise to a downstream transcription anti-terminator hairpin following P1 (Fig. 2*c*, *top*). This conformation favors polymerase readthrough, leading to full-length transcripts encoding the MntP (YoaB) efflux pump that confers Mn^{2+} resistance. Conversely, the L3 sensor loop melts in the Mn^{2+}-free state, favoring intrinsic terminator formation (Fig. 2*c*, *bottom*) that leads to premature *mntP* termination. Similar conformational changes are envisioned for translational control, although the details of these changes are unclear at present.

NiCo riboswitches confer heavy metal resistance by sensing Ni^{2+} or Co^{2+}

Heavy metals (*i.e.* $\rho > 5$ g/cm^3 (39)) such as copper and silver have long been known to possess antimicrobial properties (54). Even essential metals at sufficiently high concentrations can be toxic, as is the case for trace nutrients Ni^{2+} and Co^{2+}. These ions can be incorporated into Fe-S proteins, leading to lethal effects that necessitate strict cellular control over their uptake

(39, 55). *E. coli* senses Ni^{2+} and Co^{2+} as repellants (56) and maintains intracellular levels in the low- to sub-μM range (57). In minimal media, growth of *E. coli* is inhibited at 8 μM Ni^{2+}, and 160 μM Co^{2+} arrests *S. enterica* (58, 59). Whereas Co^{2+} is used for carbon rearrangements in the context of coenzyme B_{12}, Ni^{2+} is needed for enzymes such as hydrogenase and urease (24). Once inside the periplasm, ABC transporters and NiCo permeases are the major modes of bringing Ni^{2+} and Co^{2+} into the bacterial cell (24). The non-specific CorA transporter also facilitates cytosolic accumulation (27). To attain homeostasis, bacteria have cadmium-zinc-cobalt (*czc*) genes that encode efflux pumps and cation diffusion facilitators such as CzcD. Like the Mg^{2+}-I and Mn^{2+} riboswitches, comparative sequence analysis revealed a structured RNA motif upstream of *czcD* genes in multiple bacterial species (16). Isolated *czc* RNA motifs showed *in vitro* $K_{D,\ app}$ values of 5.6 and 12 μM for Co^{2+} and Ni^{2+}, with five metal-responsive regions in the four-way helical junction core. Comparatively weaker binding ($K_{D,\ app}$ of 220 μM) was seen for Mn^{2+}.

The *czc* motif or "NiCo" riboswitch must selectivity bind Co^{2+} or Ni^{2+} amid much higher intracellular Mg^{2+} concentrations. To elucidate the basis of affinity and recognition of these ions, a riboswitch structure was determined in the presence of Co^{2+} (16). Like the Mg^{2+}-I and Mn^{2+} riboswitches, the NiCo structure lacks pseudoknot interactions and exhibits close packing, whereby four helices coaxially stack in pairs (Fig. 3*a*). Three co-planar Co^{2+}-binding sites (I–III) reside at the interface between L2-3 and L4-1 with a fourth site (IV) at the base of P2. Like the Mn^{2+} riboswitch motif, Co^{2+} or Ni^{2+} selectivity is conferred by the purine N7 moiety, with sites I–III each coordinating two imines (Fig. 3*b*). Hill coefficients of 2.0 and 1.6 were measured for Co^{2+} and Ni^{2+}, using the *Clostridium botulinum* NiCo riboswitch. The structure nicely explains such positive cooperativity in that sites I and II coordinate the N7 and 2′-OH groups from opposing L4-1 and L2-3 nucleotides that knit the junction together. In this manner, the G46 N7 group coordinates site II, and its 2′-OH coordinates site I; conversely, the N7 group of G87 coordinates site I, and its 2′-OH coordinates sites II (Fig. 3*b*). As such, Co^{2+} binding at one site stabilizes coordination at the adjoining site. N7-deaza substitutions at G87 and G88 underscore the importance of N7 coordination. The former mutation cannot support Co^{2+}-dependent stabilization at G46, indicating that sites I and II are indeed linked. In contrast, N7-deaza G87 did not affect site III, consistent with its distal location from site I. At present, site IV appears to provide stabilization of P1-P2, with the site exhibiting a significantly lower anomalous signal than sites I–III (16).

Inspection of the NiCo riboswitch expression platform suggests the formation of two mutually exclusive conformations. At low Co^{2+} or Ni^{2+} concentrations, an intrinsic terminator hairpin is favored, whereas elevated ion levels support polymerase read-through leading to *czcD* expression (Fig. 3*c*). This mechanism was confirmed by *in vitro* transcription assays, which yielded full-length products only in the presence of cognate effector ions. Regulation was validated *in vivo* when a representative *czc* motif from *Clostridium scindens* was placed upstream of a putative cation efflux gene. Whereas levels of the associated mRNA increased with increasing Ni^{2+}, a similar analysis using non-cognate ions did not affect downstream transcript levels (16). Overall, the cooperative binding and unique mode of metal recognition by the NiCo riboswitch impart high selectivity, enabling feedback to minute changes in Co^{2+} or Ni^{2+} in a milieu of competing cellular ions to confer heavy-metal resistance. Notably, NiCo riboswitches are present in *Listeria monocytogenes*, a common foodborne pathogen (60) that is of concern because of the identification of multi-antibiotic resistance isolates in "ready-to-eat" foods (61).

Fluoride riboswitches require Mg^{2+} to sense and regulate export of a cellular toxin

Fluorine is the most electronegative and reactive element and is found predominantly in the biosphere as the fluoride ion (F^-). Although a trace element, fluorine is ubiquitous with levels ranging from 1.2 ppm (mg/liter) in seawater to 200 ppm in some soils (62, 63). High levels of F^- are toxic to bacteria, fungi, and animals (62, 64, 65), and in many regions F^- is added at 0.7 ppm to municipal water supplies as an anticaries agent (66). The beneficial and toxic effects of F^- arise from similarities in its charge and radius to hydroxide (67). The distinct antimicrobial properties of F^- are derived from its affinity for divalent cations. F^- is toxic to enolase because it stabilizes a *bis*-Mg-F-PO_4 complex that mimics the reaction intermediate (68–70). MgF_3^- and AlF_3 complexes also form trigonal-bipyramidal mimics of phosphoryl-transfer transition states (71) to inhibit catalysis by this essential class of enzymes.

Chronic contact with F^- contributed to the evolution of fluoride toxicity-resistance factors that stimulate expression of genes to ameliorate intracellular F^- levels, including transporters (19, 72–74). The observation that many bacteria and archaea use fluoride-responsive RNAs to regulate such genes suggests that F^--sensing riboswitches arose as part of an ancient strategy to achieve F^- resistance (19, 75). Such riboswitches were first identified as conserved, non-coding motifs upstream of genes such as *crcB,* which encodes a fluoride-specific channel (19, 72, 73), as well as metabolic enzymes such as enolase (19, 76). Biochemical experiments on the ~80-nucleotide *crcB* 5′-leader RNA confirmed a 1:1 binding stoichiometry for F^- only in the presence of Mg^{2+} ($K_{D,\ app}$ ~60–135 μM) (19, 77), with no apparent binding to Cl^-, Br^-, I^-, or the infused gases CO and NO. Mutations that alter conserved core sequences or secondary structures of the riboswitch adversely impact F^- binding, as expected for molecular determinants that evolved to bind a specific effector (78). Fusion of the *Bacillus cereus* 5′-leader of *crcB* to a *lacZ* reporter in *B. subtilis* revealed F^--dependent β-galactosidase activity consistent with its modulation of an intrinsic transcription terminator. Evidence for translational control by an alternative expression platform came from a *crcB* riboswitch from *Pseudomonas syringae* that lies upstream of *eriC* genes. This riboswitch was used to control *lacZ* in an *E. coli crcB* knock-out strain that is ~200-fold more sensitive to F^- than WT (19). This work demonstrated a role for CrcB in reducing cellular F^- levels and provided insight into *eriC* function and selectivity. Specifically, $EriC^F$ proteins rescued growth of *E. coli crcB* knock-out cells under high F^- conditions, suggesting that these genes are func-

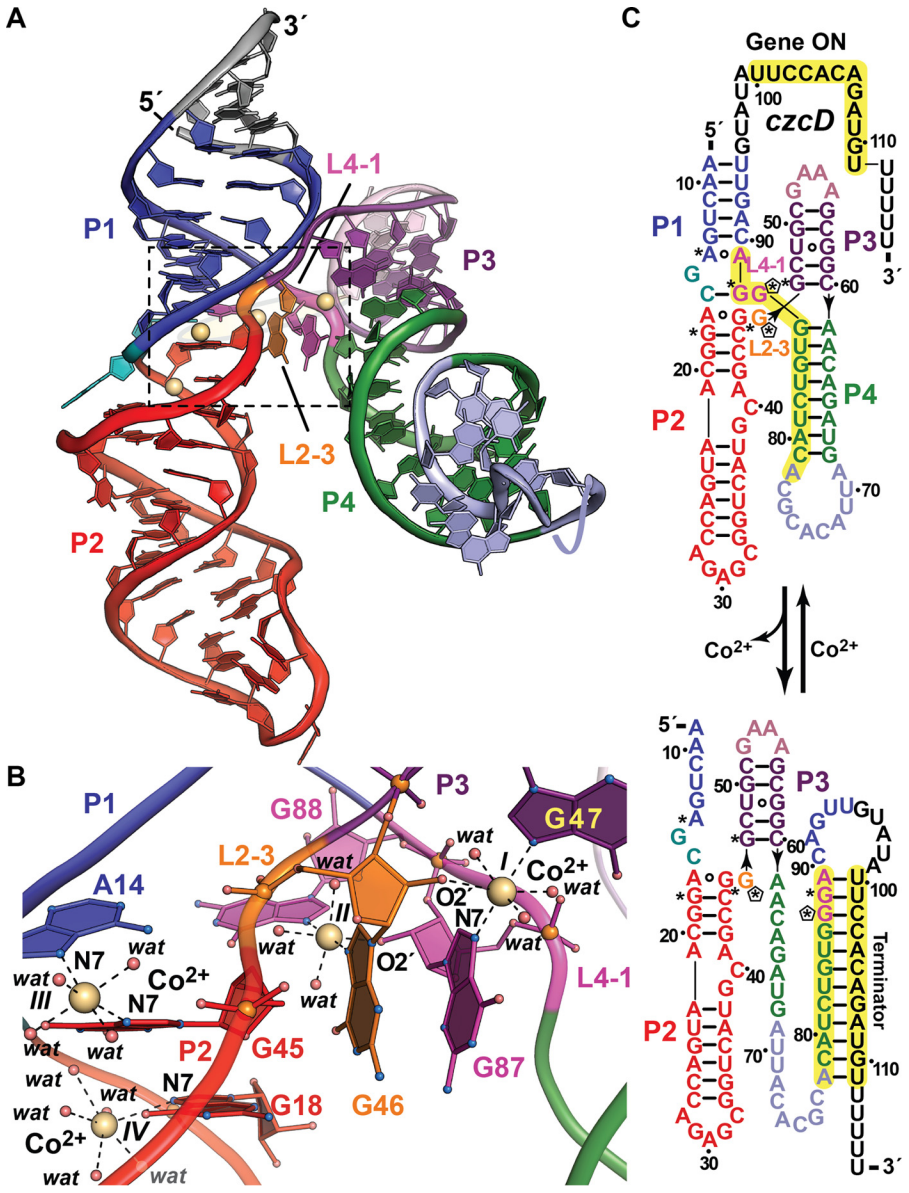

Figure 3. Tertiary fold and ion coordination by the NiCo riboswitch bound to Co^{2+}. *a,* ribbon diagram of the *Erysipelotrichaceae bacterium* riboswitch co-crystal structure determined at 2.64 Å resolution (Protein Data Bank entry 4RUM). The overall architecture comprises tandem, coaxially stacked P1-P2 and P3-P4 helices offset by 30° and joined by a central four-way helical junction. Like the Mg^{2+}-I and Mn^{2+} riboswitches, divalent ion sensing occurs at the junction interface. Here, four Co^{2+} sites (I–IV, *yellow spheres*) bind between loops L2–3 and L4–1. *b,* close-up view of the divalent ion-binding positions (*boxed* in *a*). Sites I–III interact directly with bases G47 and G87, G46 and G88, and A14 and G45, which are conserved among most *czc* homologs. G46 and G87 each contribute to coordination at sites I and II via purine N7 and ribose hydroxyl groups that form the basis of cooperativity during Co^{2+} or Ni^{2+} binding. In contrast to the Mg^{2+}-I and Mn^{2+} riboswitches that make use of non-bridging phosphate oxygens to coordinate Mg^{2+} or Mn^{2+}, NiCo riboswitch coordination utilizes one or two N7 moieties, 2′-OH groups, and water molecules to bind Co^{2+} and presumably Ni^{2+}. *c,* secondary-structure diagram depicting effector-dependent conformational changes that regulate transcription; *asterisks* indicate sites of purine N7 Co^{2+} coordination in *b*, and *pentagons* show coordination from ribose 2′-OH groups. Transcriptional regulation by the NiCo riboswitch parallels that of the Mn^{2+} riboswitch because Co^{2+} or Ni^{2+} sensing favors an RNA fold that allows RNA polymerase to read through the transcript, leading to a full-length message that confers heavy-atom resistance when translated. In the effector-free state, P4 remodels to form a terminator hairpin leading to premature transcription termination, potentially resulting in Co^{2+} or Ni^{2+} accumulation in the cell.

tionally homologous (19). Accordingly, it is now established that $EriC^F$ proteins are fluoride-selective antiporters (19, 74).

To elucidate the mode of F^- sensing and the underlying basis for gene regulation, the structure of a fluoride riboswitch was determined (77). The structure confirmed that the conserved aptamer folds as an HL_{out} pseudoknot (Fig. 4*a*) (79). Unexpectedly, a constellation of five backbone phosphates at the topological confluence of P2, L1, and L3 chelate three Mg^{2+} ions crucial for F^- sensing. These cations form the vertices of a nearly equilateral triangle with a central cavity that is ideal for F^- coordination (radius 1.30 Å) (Fig. 4*b*), while selectively excluding larger halides such as Cl^- (radius 1.81 Å) (80). Similar tri-Mg^{2+} coordination of F^- has been observed previously in proteins (81, 82).

The gene regulatory functions of *Thermotoga petrophila* and *B. cereus* fluoride riboswitches likely entail modulation of an intrinsic terminator that forms at low F^- concentration (Fig. 4*c*), ostensibly reducing CrcB levels. NMR data corroborate F^--dependent compaction of the *T. petrophila crcB* motif with interconversion of the effector free state into a compact form

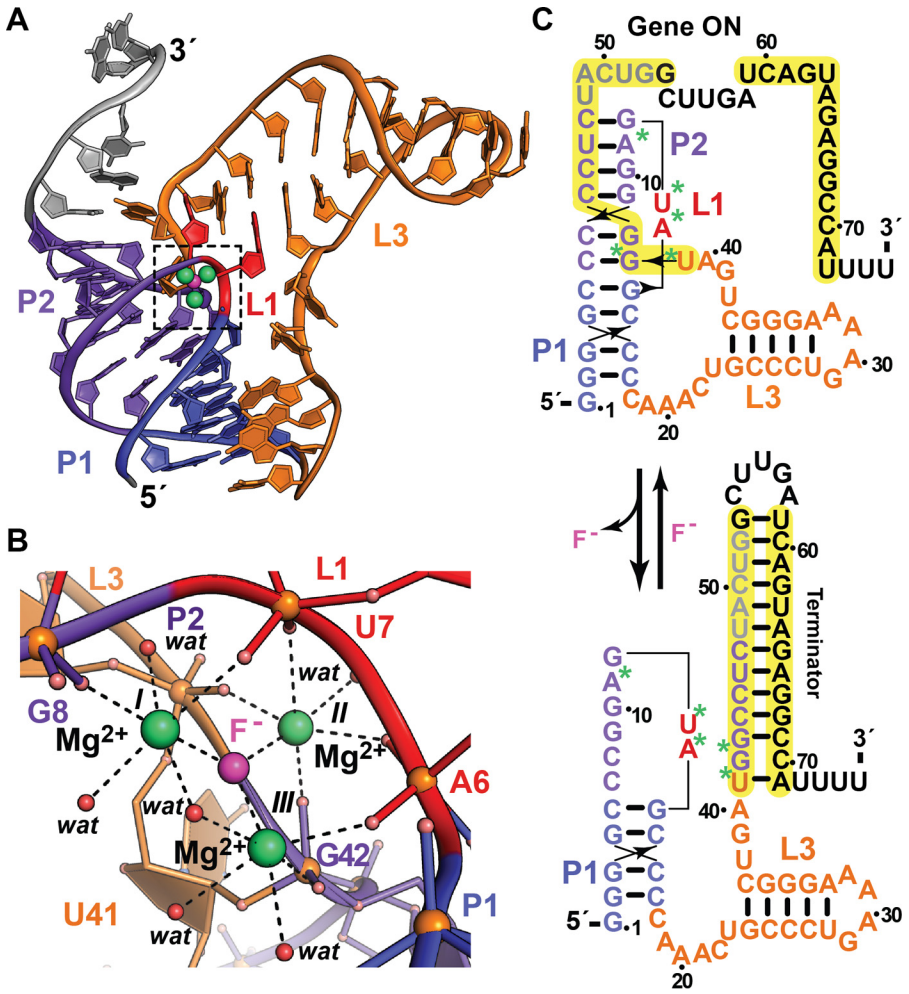

Figure 4. Tertiary fold and ion coordination by the fluoride riboswitch in complex with magnesium fluoride. *a,* ribbon diagram of the *T. petrophila* riboswitch co-crystal structure determined at 2.3 Å resolution (Protein Data Bank entry 4ENC). The riboswitch folds as an HL_{out} pseudoknot wherein F^- ion (*pink*) sensing occurs by three Mg^{2+} ions (*green*) coordinated between loops L1 and L3 that mediate long-range contacts between coaxially stacked helices P1 and P2; loop L2 = 0. *b,* close-up view of the ion-sensing pocket (*boxed* in *a*), revealing a trigonal constellation of octahedrally coordinated Mg^{2+} ions, I–III, which share a central F^- ion. Like the Mg^{2+}-I and Mn^{2+} riboswitch, non-bridging phosphate oxygens provide coordination sites for Mg^{2+} with inner-sphere water molecules completing the coordination sphere. *c,* secondary-structure diagram depicting effector-dependent conformational changes that regulate transcription; *asterisks* indicate the sites of backbone oxygen coordination to Mg^{2+} in *b*. In the presence of fluoride, the 5′-end of a terminator hairpin is buried by the pseudoknot, leading to transcription of a full-length message and translation of a CrcB channel that exports F^- to confer resistance. In the absence of fluoride, there is no need for F^- export, and the intrinsic terminator hairpin is favored, leading to the gene being maintained in an off state.

(77). Mapping the Mg^{2+} coordination sites onto the riboswitch structure suggests that structurally disparate regions in L1, P2, and L3 may be pre-organized early in transcription to coordinate F^- and Mg^{2+}, which promotes complete folding of P2 before the 5′-end of the terminator helix folds into a hairpin that arrests transcription. An alternative expression platform has been identified in the F^- riboswitch from *P. syringae* in which a Shine-Dalgarno sequence in the 3′-tail is sequestered from the 16S rRNA of the ribosome under low F^- levels (19), thus attenuating translation initiation required for $EriC^F$ synthesis.

Prospects for therapeutic targeting and discovery of new metalloriboswitches

A handful of riboswitches are known to bind metabolite analogs that alter gene expression and bacterial growth (6–9, 83, 84). Although metalloriboswitches do not bind organic ligands, they are expected to be susceptible to small molecules that target conserved binding pockets (85). Such small molecules will likely hit other members of the same class, and any escape mutant will impede normal ion binding and gene regulation. High-throughput and fragment-based screening, as well as structure-guided methods, have yielded compounds that target metabolite-sensing riboswitches (6–9, 83, 86, 87), and these approaches will likely succeed for metalloriboswitches. Small molecules that lock the Mg^{2+}-I riboswitch into a compact gene-off state (*e.g.* Fig. 1*a*) would attenuate MgtE expression, depriving bacteria of Mg^{2+}. Deletion of *mgtE* in *B. subtilis* yielded a defect requiring >25 mM Mg^{2+} for growth; by contrast, *mgtA* deletion– controlled by some Mg^{2+}-II riboswitches– had no effect (88).

As for the Mn^{2+} and NiCo riboswitches, these regulators are important when iron is scarce or H_2O_2 is present, such as inside a host cell. Therein, iron enzymes of the pathogen can lose activity, and Mn^{2+} import by MntH becomes essential (45, 89). Stabilizing the *mntH* riboswitch in a gene-off state could reduce virulence, although the details of this conformation are unclear.

Similarly, small molecules that fix the *mntP* riboswitch in a gene-on state (Fig. 2*a*) would also lower Mn^{2+} levels. Importantly, heavy metals can enter bacteria by non-specific import that requires regulated export for homeostasis (90). Whereas the *czcD* gene confers Co^{2+} and Ni^{2+} resistance, its deletion in *Streptococcus pneumoniae* led to increased Zn^{2+} sensitivity (IC_{50} of ~250 μM) (91). Zn^{2+} varies in human tissues from 20 μM in serum to 230 μM in lung (92), and high levels can impair iron enzymes by mismetallation (93). It is conceivable that trapping the NiCo riboswitch in a gene-off state (Fig. 3*c*) would impair growth under certain environmental conditions (91).

Deletion of *crcB* increases bacterial sensitivity to F^- (19), but certain compounds are also known to enhance F^- sensitivity (94–96). This work supports the prospect of targeting F^- riboswitches in concert with supplemental F^- (75). Such molecules would be selected to promote gene-off states (Fig. 4*c*), blocking F^- export. Beyond bacteria, CrcB homologs confer F^- resistance in fungi and yeast (73) but are absent in mammals. In general, F^- riboswitches are missing in eukaryotes (11), supporting prospects for antibacterial development. Overall, the metalloriboswitch field would benefit greatly by placing greater emphasis on analysis in the context of infectious disease models.

The abundance of representatives for various riboswitch classes obeys a power-law relationship that suggests ~1000 new classes remain to be discovered (11). In terms of new metalloriboswitches, it is reasonable to consider that magnesium, calcium, manganese, iron, cobalt, copper, and zinc are essential for most life forms, whereas vanadium, nickel, and tungsten are present only in bacteria (97). Each metal represents a likely effector, but it is reasonable to expect new riboswitches will sense the known ions described here. Such aptamers might possess unique sequences or use known scaffolds with variations to alter specificity (98). For example, the Mg^{2+}-I riboswitch might be co-opted to bind softer metals by replacing its oxygen ligands with nitrogen. Conversely, adding an equatorial oxygen ligand could favor pentagonal bipyramidal coordination of Ca^{2+}, which is maintained at 100–300 nM in bacteria (99). Perhaps the most likely effector is iron because it is the fourth most abundant element in the earth's crust and is essential for most life. A precedent exists for small RNA regulation of iron-storage proteins in bacteria (100). Overall, the discovery of new and possibly rare metalloriboswitches will require traditional bioinformatic methods along with targeted searches (30). All evidence suggests that the number of metal-sensing RNAs will continue to grow (11) and that this niche of genetic control is worth further consideration on the path to restoring a waning antimicrobial armamentarium.

References

1. Breaker, R. R. (2011) Prospects for riboswitch discovery and analysis. *Mol. Cell* **43,** 867–879
2. Serganov, A., and Nudler, E. (2013) A decade of riboswitches. *Cell* **152,** 17–24
3. Sherwood, A. V., and Henkin, T. M. (2016) Riboswitch-mediated gene regulation: novel RNA architectures dictate gene expression responses. *Annu. Rev. Microbiol.* **70,** 361–374
4. Breaker, R. R. (2012) Riboswitches and the RNA world. *Cold Spring Harb. Perspect. Biol.* **4,** a003566
5. Roth, A., and Breaker, R. R. (2009) The structural and functional diversity of metabolite-binding riboswitches. *Annu. Rev. Biochem.* **78,** 305–334
6. Blount, K. F., Megyola, C., Plummer, M., Osterman, D., O'Connell, T., Aristoff, P., Quinn, C., Chrusciel, R. A., Poel, T. J., Schostarez, H. J., Stewart, C. A., Walker, D. P., Wuts, P. G., and Breaker, R. R. (2015) Novel riboswitch-binding flavin analog that protects mice against *Clostridium difficile* infection without inhibiting cecal flora. *Antimicrob. Agents Chemother.* **59,** 5736–5746
7. Howe, J. A., Wang, H., Fischmann, T. O., Balibar, C. J., Xiao, L., Galgoci, A. M., Malinverni, J. C., Mayhood, T., Villafania, A., Nahvi, A., Murgolo, N., Barbieri, C. M., Mann, P. A., Carr, D., Xia, E., *et al.* (2015) Selective small-molecule inhibition of an RNA structural element. *Nature* **526,** 672–677
8. Howe, J. A., Xiao, L., Fischmann, T. O., Wang, H., Tang, H., Villafania, A., Zhang, R., Barbieri, C. M., and Roemer, T. (2016) Atomic resolution mechanistic studies of ribocil: a highly selective unnatural ligand mimic of the *E. coli* FMN riboswitch. *RNA Biol.* **13,** 946–954
9. Lee, E. R., Blount, K. F., and Breaker, R. R. (2009) Roseoflavin is a natural antibacterial compound that binds to FMN riboswitches and regulates gene expression. *RNA Biol.* **6,** 187–194
10. Ott, E., Stolz, J., Lehmann, M., and Mack, M. (2009) The RFN riboswitch of *Bacillus subtilis* is a target for the antibiotic roseoflavin produced by *Streptomyces davawensis*. *RNA Biol.* **6,** 276–280
11. McCown, P. J., Corbino, K. A., Stav, S., Sherlock, M. E., and Breaker, R. R. (2017) Riboswitch diversity and distribution. *RNA* **23,** 10.1261/rna.061234.117
12. Wang, J. X., Lee, E. R., Morales, D. R., Lim, J., and Breaker, R. R. (2008) Riboswitches that sense *S*-adenosylhomocysteine and activate genes involved in coenzyme recycling. *Mol. Cell* **29,** 691–702
13. Li, S., Hwang, X. Y., Stav, S., and Breaker, R. R. (2016) The *yjdF* riboswitch candidate regulates gene expression by binding diverse azaaromatic compounds. *RNA* **22,** 530–541
14. Breaker, R. R., Atilho, R. M., Malkowski, S. N., Nelson, J. W., and Sherlock, M. E. (2017) The biology of free guanidine as revealed by riboswitches. *Biochemistry* **56,** 345–347
15. Dann, C. E., 3rd, Wakeman, C. A., Sieling, C. L., Baker, S. C., Irnov, I., and Winkler, W. C. (2007) Structure and mechanism of a metal-sensing regulatory RNA. *Cell* **130,** 878–892
16. Furukawa, K., Ramesh, A., Zhou, Z., Weinberg, Z., Vallery, T., Winkler, W. C., and Breaker, R. R. (2015) Bacterial riboswitches cooperatively bind Ni^{2+} or Co^{2+} ions and control expression of heavy metal transporters. *Mol. Cell* **57,** 1088–1098
17. Price, I. R., Gaballa, A., Ding, F., Helmann, J. D., and Ke, A. (2015) Mn^{2+}-sensing mechanisms of *yybP-ykoY* orphan riboswitches. *Mol. Cell* **57,** 1110–1123
18. Dambach, M., Sandoval, M., Updegrove, T. B., Anantharaman, V., Aravind, L., Waters, L. S., and Storz, G. (2015) The ubiquitous *yybP-ykoY* riboswitch is a manganese-responsive regulatory element. *Mol. Cell* **57,** 1099–1109
19. Baker, J. L., Sudarsan, N., Weinberg, Z., Roth, A., Stockbridge, R. B., and Breaker, R. R. (2012) Widespread genetic switches and toxicity resistance proteins for fluoride. *Science* **335,** 233–235
20. Nierhaus, K. H. (2014) Mg^{2+}, K^+, and the ribosome. *J. Bacteriol.* **196,** 3817–3819
21. Draper, D. E., Grilley, D., and Soto, A. M. (2005) Ions and RNA folding. *Annu. Rev. Biophys. Biomol. Struct.* **34,** 221–243
22. Sigel, R. K., and Pyle, A. M. (2007) Alternative roles for metal ions in enzyme catalysis and the implications for ribozyme chemistry. *Chem. Rev.* **107,** 97–113
23. Schuwirth, B. S., Borovinskaya, M. A., Hau, C. W., Zhang, W., Vila-Sanjurjo, A., Holton, J. M., and Cate, J. H. (2005) Structures of the bacterial ribosome at 3.5 Å resolution. *Science* **310,** 827–834
24. Ma, Z., Jacobsen, F. E., and Giedroc, D. P. (2009) Coordination chemistry of bacterial metal transport and sensing. *Chem. Rev.* **109,** 4644–4681
25. Ramesh, A., and Winkler, W. C. (2010) Magnesium-sensing riboswitches in bacteria. *RNA Biol.* **7,** 77–83
26. Ibarra, J. A., and Steele-Mortimer, O. (2009) *Salmonella*–the ultimate insider. *Salmonella* virulence factors that modulate intracellular survival. *Cell. Microbiol.* **11,** 1579–1586

27. Moomaw, A. S., and Maguire, M. E. (2008) The unique nature of Mg^{2+} channels. *Physiology* **23,** 275–285
28. Centers for Disease Control and Prevention (2014) Multistate outbreak of multidrug-resistant *Salmonella* Heidelberg infections linked to foster farms brand chicken (final update). http://www.cdc.gov/salmonella/heidelberg-10-13/
29. Rothrock, M. J., Jr., Ingram, K. D., Gamble, J., Guard, J., Cicconi-Hogan, K. M., Hinton, A., Jr., and Hiett, K. L. (2015) The characterization of *Salmonella enterica* serotypes isolated from the scalder tank water of a commercial poultry processing plant: recovery of a multidrug-resistant Heidelberg strain. *Poult. Sci.* **94,** 467–472
30. Cromie, M. J., Shi, Y., Latifi, T., and Groisman, E. A. (2006) An RNA sensor for intracellular Mg^{2+}. *Cell* **125,** 71–84
31. Hollands, K., Proshkin, S., Sklyarova, S., Epshtein, V., Mironov, A., Nudler, E., and Groisman, E. A. (2012) Riboswitch control of rho-dependent transcription termination. *Proc. Natl. Acad. Sci. U.S.A.* **109,** 5376–5381
32. Spinelli, S. V., Pontel, L. B., García Véscovi, E., and Soncini, F. C. (2008) Regulation of magnesium homeostasis in *Salmonella*: Mg^{2+} targets the *mgtA* transcript for degradation by RNase E. *FEMS Microbiol. Lett.* **280,** 226–234
33. Park, S. Y., Cromie, M. J., Lee, E. J., and Groisman, E. A. (2010) A bacterial mRNA leader that employs different mechanisms to sense disparate intracellular signals. *Cell* **142,** 737–748
34. Zhao, G., Kong, W., Weatherspoon-Griffin, N., Clark-Curtiss, J., and Shi, Y. (2011) Mg^{2+} facilitates leader peptide translation to induce riboswitch-mediated transcription termination. *EMBO J.* **30,** 1485–1496
35. Merino, S., Gavín, R., Altarriba, M., Izquierdo, L., Maguire, M. E., and Tomás, J. M. (2001) The MgtE Mg^{2+} transport protein is involved in *Aeromonas hydrophila* adherence. *FEMS Microbiol. Lett.* **198,** 189–195
36. Ramesh, A., Wakeman, C. A., and Winkler, W. C. (2011) Insights into metalloregulation by M-box riboswitch RNAs via structural analysis of manganese-bound complexes. *J. Mol. Biol.* **407,** 556–570
37. Wakeman, C. A., Ramesh, A., and Winkler, W. C. (2009) Multiple metal-binding cores are required for metalloregulation by M-box riboswitch RNAs. *J. Mol. Biol.* **392,** 723–735
38. Martin, J. E., Waters, L. S., Storz, G., and Imlay, J. A. (2015) The *Escherichia coli* small protein MntS and exporter MntP optimize the intracellular concentration of manganese. *PLoS Genet.* **11,** e1004977
39. Nies, D. H. (1999) Microbial heavy-metal resistance. *Appl. Microbiol. Biotechnol.* **51,** 730–750
40. Ma, Z., Faulkner, M. J., and Helmann, J. D. (2012) Origins of specificity and cross-talk in metal ion sensing by *Bacillus subtilis* Fur. *Mol. Microbiol.* **86,** 1144–1155
41. Archibald, F. S., and Duong, M. N. (1984) Manganese acquisition by *Lactobacillus plantarum*. *J. Bacteriol.* **158,** 1–8
42. Posey, J. E., and Gherardini, F. C. (2000) Lack of a role for iron in the Lyme disease pathogen. *Science* **288,** 1651–1653
43. Papp-Wallace, K. M., and Maguire, M. E. (2006) Manganese transport and the role of manganese in virulence. *Annu. Rev. Microbiol.* **60,** 187–209
44. Jabado, N., Jankowski, A., Dougaparsad, S., Picard, V., Grinstein, S., and Gros, P. (2000) Natural resistance to intracellular infections: Natural resistance-associated macrophage protein 1 (Nramp1) functions as a pH-dependent manganese transporter at the phagosomal membrane. *J. Exp. Med.* **192,** 1237–1248
45. Kehres, D. G., Zaharik, M. L., Finlay, B. B., and Maguire, M. E. (2000) The NRAMP proteins of *Salmonella typhimurium* and *Escherichia coli* are selective manganese transporters involved in the response to reactive oxygen. *Mol. Microbiol.* **36,** 1085–1100
46. Zaharik, M. L., Cullen, V. L., Fung, A. M., Libby, S. J., Kujat Choy, S. L., Coburn, B., Kehres, D. G., Maguire, M. E., Fang, F. C., and Finlay, B. B. (2004) The *Salmonella enterica* serovar typhimurium divalent cation transport systems MntH and SitABCD are essential for virulence in an $Nramp1^{G169}$ murine typhoid model. *Infect. Immun.* **72,** 5522–5525
47. Shi, Y., Zhao, G., and Kong, W. (2014) Genetic analysis of riboswitch-mediated transcriptional regulation responding to Mn^{2+} in *Salmonella*. *J. Biol. Chem.* **289,** 11353–11366
48. Li, C., Tao, J., Mao, D., and He, C. (2011) A novel manganese efflux system, YebN, is required for virulence by *Xanthomonas oryzae* pv. *oryzae*. *PLoS ONE* **6,** e21983
49. Waters, L. S., Sandoval, M., and Storz, G. (2011) The *Escherichia coli mntR* miniregulon includes genes encoding a small protein and an efflux pump required for manganese homeostasis. *J. Bacteriol.* **193,** 5887–5897
50. Veyrier, F. J., Boneca, I. G., Cellier, M. F., and Taha, M. K. (2011) A novel metal transporter mediating manganese export (MntX) regulates the Mn to Fe intracellular ratio and *Neisseria meningitidis* virulence. *PLoS Pathog.* **7,** e1002261
51. Barrick, J. E., Corbino, K. A., Winkler, W. C., Nahvi, A., Mandal, M., Collins, J., Lee, M., Roth, A., Sudarsan, N., Jona, I., Wickiser, J. K., and Breaker, R. R. (2004) New RNA motifs suggest an expanded scope for riboswitches in bacterial genetic control. *Proc. Natl. Acad. Sci. U.S.A.* **101,** 6421–6426
52. Meyer, M. M., Hammond, M. C., Salinas, Y., Roth, A., Sudarsan, N., and Breaker, R. R. (2011) Challenges of ligand identification for riboswitch candidates. *RNA Biol.* **8,** 5–10
53. Bock, C. W., Katz, A. K., Markham, G. D., and Glusker, J. P. (1999) Manganese as a replacement for magnesium and zinc: Functional comparison of the divalent ions. *J. Am. Chem. Soc.* **121,** 7360–7372
54. Lemire, J. A., Harrison, J. J., and Turner, R. J. (2013) Antimicrobial activity of metals: mechanisms, molecular targets and applications. *Nat. Rev. Microbiol.* **11,** 371–384
55. Nies, D. H. (2003) Efflux-mediated heavy metal resistance in prokaryotes. *FEMS Microbiol. Rev.* **27,** 313–339
56. Parkinson, J. S., and Houts, S. E. (1982) Isolation and behavior of *Escherichia coli* deletion mutants lacking chemotaxis functions. *J. Bacteriol.* **151,** 106–113
57. Outten, C. E., and O'Halloran, T. V. (2001) Femtomolar sensitivity of metalloregulatory proteins controlling zinc homeostasis. *Science* **292,** 2488–2492
58. Macomber, L., Elsey, S. P., and Hausinger, R. P. (2011) Fructose-1,6-bisphosphate aldolase (class II) is the primary site of nickel toxicity in *Escherichia coli*. *Mol. Microbiol.* **82,** 1291–1300
59. Barras, F., and Fontecave, M. (2011) Cobalt stress in *Escherichia coli* and *Salmonella enterica*: molecular bases for toxicity and resistance. *Metallomics* **3,** 1130–1134
60. Centers for Disease Control and Prevention. (2016) *Listeria* outbreaks. http://www.cdc.gov/listeria/outbreaks/
61. Lim, S. Y., Yap, K. P., and Thong, K. L. (2016) Comparative genomics analyses revealed two virulent *Listeria monocytogenes* strains isolated from ready-to-eat food. *Gut Pathog.* **8,** 65
62. Kanduti, D., Sterbenk, P., and Artnik, B. (2016) Fluoride: a review of use and effects on health. *Mater. Sociomed.* **28,** 133–137
63. Adler, P., Armstrong, W. D., Bell, M. E., Bhussry, B. R., Buttner, W., Cremer, H.-D., Demole, V., Ericcson, Y., Gedalia, I., Hodge, H. C., Jenkins, G. N., Jolly, S. S., Largent, E. J., Leone, N. C., Ludwig, T. G., *et al.* (1970) Fluorides and human health. World Health Organization Monograph Series, No. 59, pp. 1–115, Geneva, Switzerland
64. Arthus, M., and Gavelle, J. (1903) Effect of sodium fluoride at 1% on a yeast. *Comptes Rendus Des Seances De La Societe De Biologie Et De Ses Filiales* **55,** 1481–1483
65. Marquis, R. E., Clock, S. A., and Mota-Meira, M. (2003) Fluoride and organic weak acids as modulators of microbial physiology. *FEMS Microbiol. Rev.* **26,** 493–510
66. Abrams, S., Beltrán-Aguilar, E., Martinez-Mier, E. A., Kumar, J., Slade, G. D., and Gooch, B. (2015) Water fluoridation: safety, effectiveness and value in oral health: a symposium at the 2014 annual meeting of the American and Canadian associations for dental research. *J. Can. Dent. Assoc.* **80,** f16
67. Garcia, M. G., and Borgnino, L. (2015) in *Fluorine: Chemistry, Analysis, Function and Effects* (Preedy, V. R., ed), pp. 1–21, Royal Society of Chemistry, Cambridge, UK
68. Warburg, O., and Christian, W. (1942) Isolation and crystallisation of the fermenting process of enolase. *Biochemische Zeitschrift* **310,** 384–421

69. Qin, J., Chai, G., Brewer, J. M., Lovelace, L. L., and Lebioda, L. (2006) Fluoride inhibition of enolase: crystal structure and thermodynamics. *Biochemistry* **45,** 793–800
70. Reed, G. H., Poyner, R. R., Larsen, T. M., Wedekind, J. E., and Rayment, I. (1996) Structural and mechanistic studies of enolase. *Curr. Opin. Struct. Biol.* **6,** 736–743
71. Jin, Y., Richards, N. G., Waltho, J. P., and Blackburn, G. M. (2017) Metal fluorides as analogs for studies on phosphoryl transfer enzymes. *Angew. Chem. Int. Ed. Engl.* **56,** 4110–4128
72. Stockbridge, R. B., Robertson, J. L., Kolmakova-Partensky, L., and Miller, C. (2013) A family of fluoride-specific ion channels with dual-topology architecture. *eLife* **2,** e01084
73. Li, S., Smith, K. D., Davis, J. H., Gordon, P. B., Breaker, R. R., and Strobel, S. A. (2013) Eukaryotic resistance to fluoride toxicity mediated by a widespread family of fluoride export proteins. *Proc. Natl. Acad. Sci. U.S.A.* **110,** 19018–19023
74. Stockbridge, R. B., Lim, H. H., Otten, R., Williams, C., Shane, T., Weinberg, Z., and Miller, C. (2012) Fluoride resistance and transport by riboswitch-controlled CLC antiporters. *Proc. Natl. Acad. Sci. U.S.A.* **109,** 15289–15294
75. Breaker, R. R. (2012) New insight on the response of bacteria to fluoride. *Caries Res.* **46,** 78–81
76. Weinberg, Z., Wang, J. X., Bogue, J., Yang, J., Corbino, K., Moy, R. H., and Breaker, R. R. (2010) Comparative genomics reveals 104 candidate structured RNAs from bacteria, archaea, and their metagenomes. *Genome Biol.* **11,** R31
77. Ren, A., Rajashankar, K. R., and Patel, D. J. (2012) Fluoride ion encapsulation by Mg^{2+} ions and phosphates in a fluoride riboswitch. *Nature* **486,** 85–89
78. Montange, R. K., and Batey, R. T. (2008) Riboswitches: Emerging themes in RNA structure and function. *Annu. Rev. Biophys.* **37,** 117–133
79. Peselis, A., and Serganov, A. (2014) Structure and function of pseudoknots involved in gene expression control. *Wiley Interdiscip. Rev. RNA* **5,** 803–822
80. Shannon, R. D. (1976) Revised effective ionic-radii and systematic studies of interatomic distances in halides and chalcogenides. *Acta Cryst. A* **32,** 751–767
81. Thorsell, A. G., Persson, C., Gräslund, S., Hammarström, M., Busam, R. D., and Hallberg, B. M. (2009) Crystal structure of human diphosphoinositol phosphatase 1. *Proteins* **77,** 242–246
82. Fabrichniy, I. P., Lehtiö, L., Tammenkoski, M., Zyryanov, A. B., Oksanen, E., Baykov, A. A., Lahti, R., and Goldman, A. (2007) A trimetal site and substrate distortion in a family II inorganic pyrophosphatase. *J. Biol. Chem.* **282,** 1422–1431
83. Sudarsan, N., Cohen-Chalamish, S., Nakamura, S., Emilsson, G. M., and Breaker, R. R. (2005) Thiamine pyrophosphate riboswitches are targets for the antimicrobial compound pyrithiamine. *Chem. Biol.* **12,** 1325–1335
84. Blount, K. F., and Breaker, R. R. (2006) Riboswitches as antibacterial drug targets. *Nat. Biotechnol.* **24,** 1558–1564
85. Breaker, R. R. (2009) Riboswitches: from ancient gene-control systems to modern drug targets. *Future Microbiol.* **4,** 771–773
86. Mulhbacher, J., Brouillette, E., Allard, M., Fortier, L. C., Malouin, F., and Lafontaine, D. A. (2010) Novel riboswitch ligand analogs as selective inhibitors of guanine-related metabolic pathways. *PLoS Pathog.* **6,** e1000865
87. Matzner, D., and Mayer, G. (2015) (Dis)similar analogues of riboswitch metabolites as antibacterial lead compounds. *J. Med. Chem.* **58,** 3275–3286
88. Wakeman, C. A., Goodson, J. R., Zacharia, V. M., and Winkler, W. C. (2014) Assessment of the requirements for magnesium transporters in *Bacillus subtilis*. *J. Bacteriol.* **196,** 1206–1214
89. Anjem, A., Varghese, S., and Imlay, J. A. (2009) Manganese import is a key element of the OxyR response to hydrogen peroxide in *Escherichia coli*. *Mol. Microbiol.* **72,** 844–858
90. Nies, D. H., and Silver, S. (1995) Ion efflux systems involved in bacterial metal resistances. *J. Ind. Microbiol.* **14,** 186–199
91. Kloosterman, T. G., van der Kooi-Pol, M. M., Bijlsma, J. J., and Kuipers, O. P. (2007) The novel transcriptional regulator SczA mediates protection against Zn^{2+} stress by activation of the Zn^{2+}-resistance gene *czcD* in *Streptococcus pneumoniae*. *Mol. Microbiol.* **65,** 1049–1063
92. Versieck, J. (1985) Trace elements in human body fluids and tissues. *Crit. Rev. Clin. Lab. Sci.* **22,** 97–184
93. Gu, M., and Imlay, J. A. (2013) Superoxide poisons mononuclear iron enzymes by causing mismetallation. *Mol. Microbiol.* **89,** 123–134
94. Nelson, J. W., Plummer, M. S., Blount, K. F., Ames, T. D., and Breaker, R. R. (2015) Small molecule fluoride toxicity agonists. *Chem. Biol.* **22,** 527–534
95. Li, S., and Breaker, R. R. (2012) Fluoride enhances the activity of fungicides that destabilize cell membranes. *Bioorg. Med. Chem. Lett.* **22,** 3317–3322
96. Nelson, J. W., Zhou, Z., and Breaker, R. R. (2014) Gramicidin D enhances the antibacterial activity of fluoride. *Bioorg. Med. Chem. Lett.* **24,** 2969–2971
97. Maret, W. (2016) The metals in the biological periodic system of the elements: concepts and conjectures. *Int. J. Mol. Sci.* **17,** 66
98. Weinberg, Z., Nelson, J. W., Lünse, C. E., Sherlock, M. E., and Breaker, R. R. (2017) Bioinformatic analysis of riboswitch structures uncovers variant classes with altered ligand specificity. *Proc. Natl. Acad. Sci. U.S.A.* **114,** E2077–E2085
99. Dominguez, D. C. (2004) Calcium signalling in bacteria. *Mol. Microbiol.* **54,** 291–297
100. Massé, E., and Gottesman, S. (2002) A small RNA regulates the expression of genes involved in iron metabolism in *Escherichia coli*. *Proc. Natl. Acad. Sci. U.S.A.* **99,** 4620–4625